ChemComm

COMMUNICATION

Cite this: *Chem. Commun.*, 2018, **54**, 1861

Received 2nd November 2017,
Accepted 24th January 2018

DOI: 10.1039/c7cc08443a

rsc.li/chemcomm

Intrinsic optical sectioning with upconverting nanoparticles†

C. Sorbello and R. Etchenique *

Multiphoton microscopy is a powerful technique for imaging due to its deep penetration, low scattering and sectioning power, allowing control on all three axes for both imaging and molecular actuation, but involves expensive femtosecond lasers. We show that lanthanide-based Upconverting Nanoparticles offer an under $1000 solution with the main advantages of multiphoton imaging, including direct optical sectioning in complex 3D samples.

Multiphoton microscopies offer important advantages over their 1-photon counterparts: NIR excitation, deeper penetration in living tissue, lower scattering and *z*-axis sectioning. Among them, the direct sectioning power that arises from a nonlinear emission–excitation relationship is perhaps the most interesting one. The fact that the emission follows the square (or a superior power) of the excitation confines it to the focal zone, leaving the regions below and above the focal plane unperturbed, especially when high aperture objectives are used. Optical sectioning can also be obtained through confocal microscopy. However, while confocal techniques illuminate a full bicone of light and limit the focal plane by means of the collection optics (pinhole), multiphoton microscopies produce the very excitation only at the focal plane, preventing the rest of the sample from reaching excited states which lead to emission or further photochemical pathways. This property has two additional advantages: (a) probe photobleaching is confined to the focal zone and (b) great 3D resolution can be obtained when stimulating phototriggers.

Since Denk reported the first two-photon (2P) microscope,[1] many probes and actuators have been designed and developed for imaging[2–4] and phototriggering biological systems.[5–7] Two (or more) photon absorption is a hard way towards excitation. Most substances have negligible absorption for processes that involve more than one photon. In order to obtain a reasonable emission flux after 2P excitation, an enormous instantaneous power density must be delivered into the sample albeit keeping the average power low in order to prevent damage through overheating. Ti-Sapphire lasers are delicate, big and expensive, these being the main reasons multiphoton microscopies are not so widely extended as their advantages would suggest. In a typical application a 4 W average power Ti-Sapphire laser, with 140 fs pulses and 80 MHz repetition rate can reach a maximum power of 4.5×10^{13} W cm^{-2} at the sample.[8]

Luminescent nanoparticles are established as useful tools for imaging biological systems. Their uses range from robust probes with very high tolerance to photobleaching[9] to nanosized barcoding systems.[10] Among nanoparticles, some lanthanide-containing nanocrystals show upconversion, a photophysical process by which two or more photons of a lower energy are absorbed by a system which eventually decays through the emission of a higher energy photon.[11] Multiphoton excitation and upconversion are two quite different processes. In the first mechanism, two or more photons are absorbed quasi-simultaneously, populating the emitting excited state from the ground level. A formalism having a virtual state is often used to depict this process, as shown in Fig. 1a. Conversely, upconversion involves real, long lived excited states that lay between the ground and the emitting states, which can be

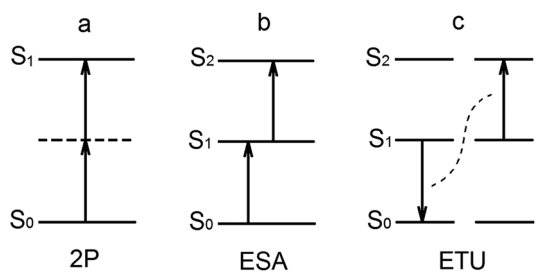

Fig. 1 Scheme of the mechanisms of multiphoton absorption and upconversion. (a) Two photon absorption, depicting the virtual state between S0 and S1. (b) Excited state absorption, showing the real intermediate state. (c) Energy transfer upconversion.

Departamento de Química Inorgánica, Analítica y Química Física, INQUIMAE, Facultad de Ciencias Exactas y Naturales, Universidad de Buenos Aires, CONICET, Ciudad Universitaria Pabellón 2, AR1428EHA Buenos Aires, Argentina.
E-mail: rober@qi.fcen.uba.ar

† Electronic supplementary information (ESI) available: The emission spectra and temporal characteristics of the UCNPs as well as the diagram of the setup used are presented. See DOI: 10.1039/c7cc08443a

populated, accumulating energy that eventually will be released as emission of a short wavelength photon. Several internal mechanisms are usually present in upconverting systems, Fig. 1b and c depict the more widely studied mechanisms: Excited State Absorption (ESA) and Energy Transfer Upconversion (ETU). The presence of these intermediate energy states has a profound effect in the absorption cross section. While usual 2P absorption needs both photons to be absorbed within the time of a transition ($\sim 10^{-15}$ s) and therefore very high instantaneous powers, upconversion mechanisms operate in the range of 10^{-5} s and can thus be efficient even at excitation powers of ten orders of magnitude lower than those required for 2P processes. High efficiency upconverting phosphors can be used not only as probes but also to uncage molecules from phototriggers which usually require UV or visible instead of NIR light.[12]

Even though the photophysics underlying upconversion is different from that of 2P absorption, the equations governing both mechanisms are essentially the same. In stationary state, the emission intensity will scale as a power of the excitation power, where the power is equal to the number of photons needed to reach the emissive excited state. Due to this fact, it is expected that upconversion microscopy would behave as conventional multiphoton microscopies, yielding *z*-axis sectioning.

However, reports on using upconverting probes to take advantage on their intrinsic sectioning capabilities are scarce and negative. Yang *et al.*[13] employed upconversion nanoparticles (UCNPs) in a scanning scheme to image labelled cells, although they have not succeeded in obtaining intrinsic sectioning, attributing this failure to the nature of upconversion mechanism and finally used a confocal pinhole to achieve z-sectioning. Van Veggel[14] has pointed out the main problem of upconversion excitation. In brief, the same characteristics that allow multiphoton absorption with high cross section at low power densities imply that the saturation of the intermediate states becomes important at rather low excitation fluxes, linearizing the effective emission-to-excitation dependence and precluding sectioning. Some authors have tried to circumvent this issue by applying confocal techniques to upconversion. This is a hard task to accomplish due to the long characteristic times of UCNP emission, which implies very low scanning sweeping speed or image smearing. Romanowsky has devised a clever procedure to reconstruct smeared images through deconvolution, useful for sparse labelling,[15] while Pierce has attacked the problem by means of line confocal microscopy,[16] where just the slow axis needs to be swept. UCNPs can also be used for sub-diffraction imaging, as demonstrated by Zhan *et al.*[17] However, these latter approaches also allow image sectioning by means of deconvolution or confocal procedures, disregarding the intrinsic sectioning power of upconversion as a nonlinear emission process.

Here we present the first demonstration of full multiphoton sectioning obtained using upconversion nanoprobes. We characterize the method, showing that the only requisite for having good sectioning power is to prevent saturation, being upconversion similar to traditional multiphoton microscopies in this respect. We measured the main optical characteristics of upconversion microscopy at different regimes. Finally, we solved the problem of having simultaneously long collection times and fast scanning by using parallel descanning through a CCD sensor. We obtained optical sections of highly homogeneously labeled specimens using a low power laser diode as light source and an overall equipment three orders of magnitude cheaper than the usual 2P microscopes. In this way, Scanning Laser Upconversion Microscopy (SLUM) opens a new path to inexpensive but precise imaging and/or manipulation of small objects.

Er-Containing UCNPs ($NaYF_4$: 2 mol% Er^{3+}: 30 mol% Yb^{3+}) were synthesized as published.[18] The details are given as ESI.† The particles present absorption at NIR ($\sim$980 nm) and anti-stokes emission at two main bands: 500–550 nm ($^4S_{3/2}$–$^4I_{15/2}$ and $^2H_{11/2}$–$^4I_{15/2}$ transitions) and 640–670 nm ($^4F_{9/2}$–$^4I_{15/2}$). Most absorption corresponds to the Yb^{3+} $^2F_{7/2}$–$^2F_{5/2}$ transition, which is the most efficient and which can populate the Er^{3+} excited states through ET, as depicted in Fig. S1 (ESI†), together with the experimental emission data. Both green and red emission bands correspond to biphotonic processes. Therefore, in absence of saturation the emission scales as the square of the excitation intensity. Upconverting emission is a rather slow process, with characteristic times in the hundreds of μs, depending on the exact composition of the UCNPs. Fig. S3 (ESI†) shows the temporal characteristics of the UCNPs used in this work. These long characteristic times imply that building up an image on a traditional sequential pixel-by-pixel basis would take about 5 minutes per frame for a typical 640 × 480 image. To accelerate acquisition we used parallel descanning using a CCD sensor. Since the optimal excitation time per sample point in our setup is around 10 μs, the total time required to excite the complete imaged area is $\sim$2.5 s. This fast scanning is key to prevent saturation of the probes and therefore keep *z*-axis sectioning while maintaining high average excitation power (*vide infra*). The microscope and camera optics direct the light from each excited point to a different sensor pixel, and all pixels can be measured at once by opening the camera shutter, scanning the NIR excitation laser over the whole imaged area while collecting the upconverted emission and then closing the shutter. With this method, emitted light is captured simultaneously, for a long time and for every excited point of the sample thus allowing for complete excitation decay without lengthening the total acquisition time. The diagram of the setup and more detail on the scanning–descanning procedure is given as ESI† (Fig. S3 and S4).

In order to evaluate the sectioning capabilities of SLUM it is convenient to image a simple object. We chose a thin homogeneous layer of UCNPs embedded in polystyrene by spin coating. For a Gaussian beam focused and swept throughout this sample, the total emission of an area patch is given by the following equation (complete derivation is given as ESI†):

$$I_{\mathrm{em}} = k\pi\left(\omega_0^2 + z^2\mathrm{NA}^2\right)^{1-n} \quad (1)$$

where k is a constant that includes all instrumental parameters and also the emission quantum yield of the probe, z is the distance from the focal plane, ω_0 (the Gaussian beam waist) is the distance at which the intensity of the beam has decreased to $1/e^2 \cong 0.135$ and n is the number of photons of the nonlinear process. For linear emission ($n = 1$) the last factor equals 1 and thus the overall emission intensity becomes independent on

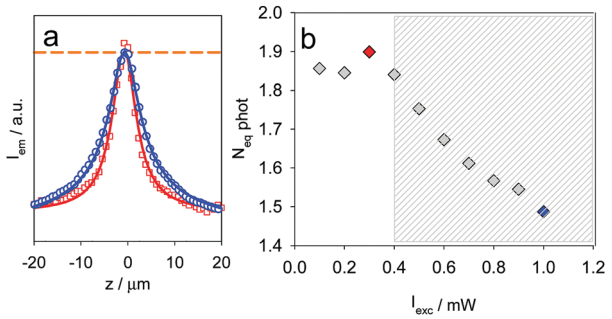

Fig. 2 (a) Performance of z-sectioning at two different excitation intensities. The specimen is an infinitely thin sheet of upconverting nanoparticles. P = 0.3 mW (red) and P = 1 mW (blue), both at an x-axis scanning speed of 9.6 cm s^{-1}. The solid lines are the best fits to the eqn (1). The orange dashed line indicates the emission expected for a linear process. (b) Dependence of the equivalent number of photons with the excitation power. The red and blue diamonds correspond to the curves in (a). The grayed zone indicates focal saturation.

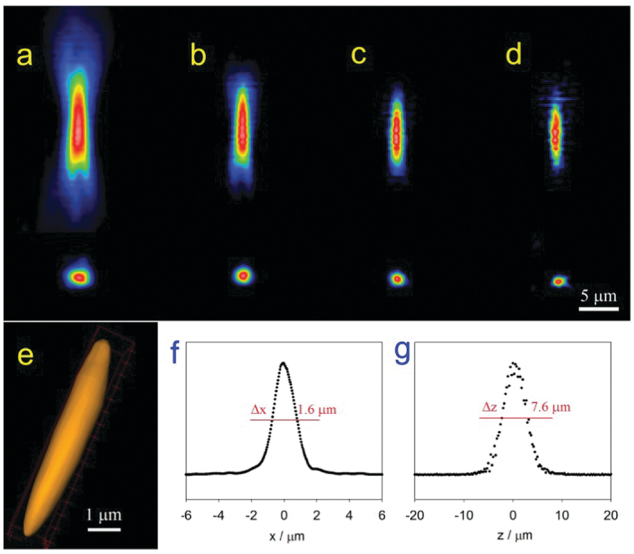

Fig. 3 (a–d) False colour images of the point spread function of SLUM (top xz plane, bottom xy plane) at different excitation intensities. (a) 3 mW, (b) 0.1 mW, (c) 25 μW, (d) 10 μW (NA = 0.65). (e) 3D reconstruction of the PSF (p = 25 μW). (f) Resolution of SLUM in lateral (x,y) directions. (g) Resolution of SLUM in axial (z) direction (p = 25 μW).

the defocus distance (no sectioning) as shown in the dashed line of Fig. 2a. For any nonlinear processes with $n > 1$ the emission intensity presents a maximum at the focal plane.

Upconversion mechanisms often provide fractional values of n, indicating the multiplicity of pathways by which the emissive state can be reached[19] and the fact that intermediate states can be saturated. The plots in Fig. 2a shown experimental data and their best fit of eqn (1) at different excitation powers, in which saturation is present (blue) or almost absent (red). Fig. 2b depicts the effective photonicity of the overall emission process for a range of excitation powers at the sample. Saturation of intermediate states appears at I_{exc} above 300 μW and increases with power.

These considerations indicate that saturation must be avoided to get good sectioning power. There are two ways to achieve this goal: to lower the excitation density or to increase the scanning speed,[20] in order to allow the probes to receive light just a very small fraction of the time. In both cases, the needed time for a given image below the saturation point will be given by the absolute sensitivity of the camera and the efficiency of the optical collection system.

The Point Spread Function (PSF) of an imaging system describes the response of this system to a point object. Any obtained image can be described as the convolution of the imaged object with the PSF of the system. Therefore, it is useful to obtain the PSF of a system as a basis for comparison.[21] To estimate the PSF of the SLUM at different saturation conditions, we have focused a stationary beam on a thin layer of UCNPs, forming an emitting object with negligible size in z-direction and near-Gaussian profile in x and y directions. The obtained raw images were deconvolved with the estimated size of the emitting object and the results at different excitation intensities are depicted in Fig. 3.

Most importantly, while the excitation power does not substantially change the on-plane resolution (x,y), it has a profound effect in the axial (z) direction. At high excitation density, saturation of intermediate states allows the emitters to absorb and emit through a 1-photon mechanism. Under this regime the sectioning power of the SLUM vanishes, showing the bi-conical excitation as a normal epifluorescence microscope.

On the contrary, at lower intensities, nonlinear multiphoton regime takes place and the PSF shows the typical z-localized ovoid shape of 2P microscopies. For excitation densities below 25 μW (~1200 W cm^{-2}) and using an NA = 0.65 objective, the lateral resolution is Δx = 1.6 μm and the axial resolution is Δz = 7.6 μm.

The differences with the theoretical values for a perfectly focused Gaussian beam (Δx = 0.9 μm and Δz = 6.9 μm respectively) can be ascribed to aberrations and slight misalignment of the optical system.

In order to show the power of the technique, we have chosen a suitable specimen to compare z-sectioning: a pollen grain (*Abutilon grandifolium*) covered with UCNPs forming an homogeneous layer of emitters rather than a sparse one, which would be difficult to separate using deconvolution techniques.

Fig. 4 shows a series of images of the specimen imaged at different planes with the same optics but varying the parameters in order to obtain linear or multiphoton images. Seven of these image planes are depicted in the panel (a). The row (b) shows the specimen as seen through bright field (λ = 525 nm) at the chosen focused planes. As usual, out-of-focus light obscures the fine details of the specimen. Linear emission microscopy is not capable to solve this issue: the row (c) shows the image under Koehler epi-illumination, where NIR (980 nm) excitation intensity independent on the z position. Although the upconverted emission is a multiphoton process, as the excitation density does not change at different planes, the overall effect is the same as if where imaged by means of conventional 1-photon fluorescence, as usual in upconversion microscopies. The collected emission of every plane throughout the sample has a similar brightness,

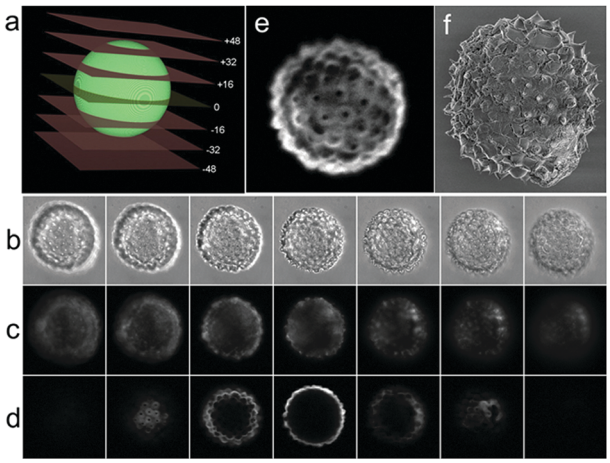

Fig. 4 Pollen grain (*Abutilon grandifolium*) covered with UCNPs, immersed into ethyl salicylate and imaged by means of different techniques: (a) scheme of the depicted focal planes in panels (b–d). Distances from the equatorial plane are given in μm. (b) Bright field images illuminated with a 525 nm LED source. (c) Linear epi-illumination images of the same specimen using a non focused 980 nm laser diode excitation. (d) SLUM images at p = 500 μW, v = 19.2 cm s^{-1} of the same specimen showing 2-P sectioning power. All images were taken through a 40 × 0.65 objective. (e) 3D reconstruction of the pollen grain. (f) SEM image of the pollen grain in vacuum.

which is given by the excitation intensity. Therefore, the out of focus light also prevents any fine structure of the grain to be distinguished. On the other hand, the sectioning power of SLUM is clearly depicted in Fig. 4d: the images were taken with p = 0.5 mW excitation power at a scanning speed of 19.2 cm s^{-1}. At this speed, and considering the PSF, the focal volume is excited during about 8.3 μs during the beam flight. The equatorial image shows that the non labelled interior of the grain is clearly observed, even through the bright exine capsule. However, for higher excitation power the intermediate states of the emitters are highly populated and the sectioning power of the technique vanishes. Fig. S5 (ESI†) shows a comparison of the pollen grain taken at three different excitation intensities.

A reconstructed 3D view of the pollen grain is also shown (Fig. 4e), in complete accordance with the image obtained by SEM (Fig. 4f). While the SEM picture is somewhat distorted due to the high vacuum needed to image it, the 3D reconstruction preserves the near spherical shape. It is important to emphasize that the observed sectioning was not obtained by means of eliminating off-focus light as in confocal procedures, but due to the intrinsic nonlinear nature of the involved process.

This fact indicates that the same strategy used to achieve true 3D localized excitation can be used to elicit photochemical responses (*i.e.* drug uncaging,[22] nanopatterning,[23] photodynamic therapy,[24] *etc.*) in thick systems, as is usual with standard 2P techniques.

In conclusion, we have shown that true z-sectioning can be performed using upconverting nanoparticles as probes. The key of this achievement rests on the use of very low duty cycle excitation pulses thus preventing saturation of the intermediate states of the UCNPs, and keeping the emission in nonlinear multiphoton regime. This method presents figures of merit near to the theoretical ones for the particular optics used and allows the construction of a very low cost 2P microscope, where solid-state laser diodes replace the bulky and expensive Ti-Sapphire femtosecond oscillators. We have tested a simple version of such microscope as a proof of concept to show sectioning in a spheroidal pollen grain. Given that the multiphoton sectioning is intrinsic to the nonlinear excitation mechanism, the same technique may be used to perform photolithography, uncaging, drug delivery, 3D photopatterning, depth localized photodynamic therapies, *etc.*, opening a wide field of low cost and small-sized methods for sensing and actuating with exquisite 3D resolution.

We gratefully thank Dr Oscar Filevich for fruitful discussions. This research was supported by the National Agency for Science and Technology Promotion, CONICET, and the University of Buenos Aires C. S and R. E. are members of CONICET.

Conflicts of interest

There are no conflicts to declare.

Notes and references

1 W. Denk, J. H. Strickler and W. W. Webb, *Science*, 1990, **248**, 73–76.
2 V. Nikolenko, K. E. Poskanzer and R. Yuste, *Nat. Methods*, 2007, **4**, 943–950.
3 K. Svoboda and R. Yasuda, *Neuron*, 2006, **50**, 823–839.
4 E. Chaigneau, M. Oheim, E. Audinat and S. Charpak, *Proc. Natl. Acad. Sci. U. S. A.*, 2003, **100**, 13081–13086.
5 B. Judkewitz, A. Roth and M. Häusser, *Neuron*, 2006, **50**, 180–183.
6 R. Araya, V. Andino-Pavlovsky, R. Yuste and R. Etchenique, *ACS Chem. Neurosci.*, 2013, **4**, 1163–1167.
7 L. Donato, A. Mourot, C. M. Davenport, C. Herbivo, D. Warther, J. Léonard, F. Bolze, J. F. Nicoud, R. H. Kramer, M. Goeldner and A. Specht, *Angew. Chem., Int. Ed.*, 2012, **51**, 1840–1843.
8 D. G. Rosenegger, C. H. T. Tran, J. LeDue, N. Zhou and G. R. Gordon, *PLoS One*, 2014, **9**, e110475.
9 P. Rees, J. W. Wills, M. R. Brown, J. Tonkin, M. D. Holton, N. Hondow, A. P. Brown, R. Brydson, V. Millar, A. E. Carpenter and H. D. Summers, *Nat. Methods*, 2014, **11**, 1–7.
10 O. S. Wolfbeis, *Chem. Soc. Rev.*, 2015, **44**, 4743–4768.
11 B. Zhou, B. Shi, D. Jin and X. Liu, *Nat. Nanotechnol.*, 2015, **10**, 924–936.
12 A. E. Pierri, P.-J. Huang, J. V. Garcia, J. G. Stanfill, M. Chui, G. Wu, N. Zheng and P. C. Ford, *Chem. Commun.*, 2015, **51**, 2072–2075.
13 M. Yu, F. Li, Z. Chen, H. Hu, C. Zhan, H. Yang and C. Huang, *Anal. Chem.*, 2009, **81**, 930–935.
14 J. Pichaandi, J. C. Boyer, K. R. Delaney, F. C. J. M. Van Veggel and F. C. J. M. van Veggel, *J. Phys. Chem. C*, 2011, **115**, 19054–19064.
15 C. F. Gainer, U. Utzinger and M. Romanowski, *J. Biomed. Opt.*, 2012, **17**, 76003.
16 L. M. Higgins, M. Zevon, V. Ganapathy, Y. Sheng, M. C. Tan, R. E. Riman, C. M. Roth, P. V. Moghe and M. C. Pierce, *J. Biomed. Opt.*, 2015, **20**, 110506.
17 Q. Zhan, H. Liu, B. Wang, Q. Wu, R. Pu, C. Zhou, B. Huang, X. Peng, H. Ågren and S. He, *Nat. Commun.*, 2017, **8**, 1058.
18 J. C. Boyer, C. J. Carling, B. D. Gates and N. R. Branda, *J. Am. Chem. Soc.*, 2010, **132**(44), 15766–15772.
19 M. Pollnau, D. Gamelin, S. Lüthi, H. Güdel and M. Hehlen, *Phys. Rev. B: Condens. Matter Mater. Phys.*, 2000, **61**, 3337–3346.
20 J. Hodak, Z. Chen, S. Wu and R. Etchenique, *Anal. Chem.*, 2016, **88**(2), 1468–1475.
21 A. Periasamy, P. Skoglund, C. Noakes and R. Keller, *Microsc. Res. Tech.*, 1999, **47**, 172–181.
22 S. Wu and H. J. Butt, *Adv. Mater.*, 2016, **28**, 1208–1226.
23 Z. Chen, S. He, H. J. Butt and S. Wu, *Adv. Mater.*, 2015, **27**, 2203–2206.
24 N. M. Idris, M. K. Gnanasammandhan, J. Zhang, P. C. Ho, R. Mahendran and Y. Zhang, *Nat. Med.*, 2012, **18**, 1580–1585.

